Computational Aeroelastic Analysis of a Hovering W3 Sokol Blade with Gurney Flap

V.A. Pastrikakis[a,1], R. Steijl[a,2], G.N. Barakos[a,3], J. Małecki[b,4]

[a] *The University of Liverpool, CFD Laboratory, School of Engineering, Liverpool L693GH, U.K.*
[b] *PZL-ŚWIDNIK Spółka Akcyjna, Al. Lotników Polskich 1, 21-045 Świdnik, Poland*

Abstract

This paper demonstrates the potential effect of a gurney flap on the performance of the W3-Sokol rotor blade in hover. A rigid blade was first considered and the calculations were conducted at several thrust settings. The gurney flap was extended from 46%R to 66%R and it was located at the trailing edge of the main rotor blade. Four different sizes of gurney flaps were studied, 2%, 1%, 0.5% and 0.3% of the chord. The biggest flap proved to be the most effective. A second study considered elastic blades with and without the gurney flap. The results were trimmed at the same thrust values as the rigid blade and indicate an increase of aerodynamic performance when the gurney flap is used, especially for high thrust cases.

Keywords: Computational Fluid Dynamics, rotor, hover, gurney flap

URL: `http://www.liv.ac.uk/cfd` ()
[1]Ph.D. candidate, vasileios.pastrikakis@liv.ac.uk
[2]Lecturer, rsteijl@liv.ac.uk
[3]Professor, corresponding author, g.barakos@liv.ac.uk
[4]Leading Specialist for Aeromechanics and Dynamics, jacek.malecki@pzl.swidnik.pl

March 24, 2016

Nomenclature

LATIN

a	=	Lift slope
c	=	Chord in untapered part of the blade (m)
k	=	Turbulent kinetic energy
l	=	Characteristic scale of the flow (main chord at this study) (m)
v	=	Mean velocity of the blade section relative to the fluid (m/s)
a_{sound}	=	Speed of sound (m/s)
c_{P}	=	Pressure coefficient
C_{T}	=	Thrust coefficient, $C_{\text{T}} = T/(0.5\rho\pi R^2 V_{\text{tip}}^2)$
C_{Q}	=	Torque coefficient, $C_{\text{Q}} = Q/(0.5\rho\pi R^3 V_{\text{tip}}^2)$
C_{t}	=	Sectional thrust coefficient, $C_{\text{t}} = L_{\text{z}}/(0.5\rho c V_{\text{tip}}^2)$
C_{m}	=	Sectional moment coefficient, $C_{\text{m}} = L_{\text{m}}/(0.5\rho c^2 V_{\text{tip}}^2)$
C_{q}	=	Sectional torque coefficient, $C_{\text{q}} = L_{\text{q}}/(0.5\rho c^2 V_{\text{tip}}^2)$
E	=	Total iternal energy per unit mass
L_{z}	=	Rotor loading along the span in the thrust direction (N/m)
L_{m}	=	Rotor moment loading around the blade pitch axis (N)
L_{q}	=	Rotor moment loading around the shaft axis (N)
M	=	Mach number (v/a_{sound})
N_{b}	=	Number of blades
P_{i}	=	Ideal induced rotor power
P	=	Actual rotor power
R	=	Aspect ratio of the blade
$V(t)$	=	Time dependent cotrol volume
Re	=	Reynolds Number (vl/ν)
FM	=	Figure of merit, FM $= P_{\text{i}}/P$
BVI	=	Blade Vortex Interaction
MRB	=	Main Rotor Blade
CFD	=	Computational Fluid Dynamics
CVT	=	Constant Volume Tetrahedral
PIV	=	Particle Image Velocimetry
SAM	=	Spring Analogy Method
TFI	=	Transfinite Interpolation
$\vec{R}_{\text{i,j,k}}$	=	Flux residuals at cell (i, j, k)
$\vec{w}$	=	Vector of conserved variables

$\vec{F}a_{\mathrm{i}}$	=	Inviscid fluxes
$\vec{F}a_{\mathrm{v}}$	=	Viscous fluxes
$\vec{n}a_{\mathrm{i}}$	=	Normal vector of the i-th face of a cell
$\vec{S}$	=	Source term
Subscripts		
∞	=	Free-stream Value
tip	=	Tip value
GREEK		
α	=	Angle of insidence (degrees)
β or β_0	=	Flapping angle (degrees)
γ	=	Rotor blade Lock number, $(\phi\alpha cR^4/I_b)$
θ or θ_0	=	Collective angle at 75%R (degrees)
λ	=	Inflow factor
ν	=	Kinematic viscosity, $(\mu_{\mathrm{v}}/\rho,\ m^2/s)$
μ	=	Advance ratio
μ_{v}	=	Dynamic viscosity (kg/ms)
ρ	=	Density (kg/m^3)
σ	=	Rotor solidity, $(N_{\mathrm{b}}cR/\pi R^2)$
ω	=	Specific dissipation (m^2/s^3)
$\vec{\omega}$	=	Rotor rotational speed

1. Introduction

The use of gurney flaps for lift enhancement is well established in the aerospace community and several research works like the one by Wang et al. (2008) document the advantages and disadvantages of these devices. The gurney flap was introduced by race car driver Gurney and its aerodynamics were first studied by Liebeck (1978). This has been followed by numerous experimental studies conducted by Jeffrey and Zghang (2000), Troolin et al. (2006), and Lee and Su (2011). Tang and Dowell (2007) compared the loading of a NACA0012 wing section with both static and oscillating trailing-edge gurney flaps using an incompressible Navier-Stokes code against experiments conducted in a wind tunnel by them. Due to the scarcity of experimental data with dynamically deployed gurney flaps Chow and Dam (2006), Baker et al. (2007), and Kinzel et al. (2010) have utilised this set of data in their computational studies.

The gurney flap is a short flat plate placed at the trailing edge, perpendicular to the chord-line on the pressure side of the aerofoil, and works by providing a stagnation area near the trailing edge resulting in an increase of lift. It increases the zero lift angle and keeps the lift slope constant so there is a decrease in the stall angle. The pitching moment coefficient is also increased (i.e. more nose down) as presented by Gai and Palfrey (2003) and unless the gurney is sized carefully, substantial drag penalties may also occur. Based on the review of flow control mechanisms by Yeo (2008) gurney flaps are generally less than 3% of the wing chord. Previous studies by Jeffrey et al. (2000) and Maughmer and Bramesfeld (2008) have concluded that the optimal height for a gurney flap should be close to the boundary layer thickness on the pressure side of the aerofoil. If the gurney flap height is smaller than the boundary layer thickness, then its influence is significantly decreased, while increasing the size of the flap leads to a drag penalty.

Most of the studies found in the literature are dealing with commonly used aerofoils in rotorcraft applications, and try to derive conclusions concerning the potential effect of the gurney flap on rotor blades according to two-dimensional calculations, like the studies conducted by Yee et al. (2007), and Liu et al. (2011). Min et al. (2009) studied the effects of gurney flaps on the blade root loads and hub vibratory loads. In their study, a gurney flap was deployed over the entire span of the BO-105 rotor in forward flight with three different deployment schedules. A carefully chosen azimuthal deployment schedule of the gurney flap was found to reduce the peak-to-

peak variations in hub loads. The 4-per-revolution normal force at the hub was compared with the loads for a higher harmonic controlled rotor and the baseline rotor. The simulations showed that the gurney flap deployment reduced by 80% the 4-per-rev normal force vibration. For the same rotor in descending flight, a gurney set at 30 degrees angle relative to the mean chord resulted in a 40% decrease of the vertical descend rate. However, the gurney flap resulted in local nose-down pitching moment, and altered the trim condition, which indicates that additional fluid-structure coupling analysis for aeroelastic deformation and rotor trim is required.

Active gurney flaps were also studied by Padthe et al. (2011) to determine their effectiveness in reducing noise and vibration in rotorcraft, as well as improving rotor performance. Active control studies employing microflaps were conducted on a hingeless rotor configuration resembling the MBB BO-105, and various spanwise configurations of the flaps, including a single, a dual, and a segmented five-flap configuration were evaluated. Results indicate that the gurney flap is capable of substantial reductions in blade vortex interaction (BVI) noise ranging from 3-6 dB. Vibration reduction ranging from 70-90% was also demonstrated. Vibration and noise reduction was also examined at the same time, and was found that reduction in one was linked to an increase on the other. Finally, the gurney flap appeared to be more effective in reducing the BVI noise at both advancing and retreating sides while the plain flap was more effective in reducing the vibrations.

The effectiveness of a single active gurney flap in reducing vibration of a UH-60A Blackhawk helicopter in high-speed flight ($\mu = 0.35$) was studied by Bae and Gandhi (2012). An elastic blade was considered and the gurney flap was extending from 70%R to 80%R and was deployed to an amplitude of 0.5% of the chord. The gurney flap actuation was most influential in reducing the vertical vibratory hub force. The most effective actuation input was 4/rev and it led to 80% reduction.

Comparing the above studies by Min et al. (2009), Padthe et al. (2011), and Bae and Gandhi (2012), to the ones conducted by Milgram et al. (1998), and Viswamurthy and Ganguli (2004) it seems that a gurney flap can have a similar effect on the vibratory loads of the rotor hub like a conventional trailing edge flap. A typical flap is suggested by Viswamurthy and Ganguli (2004) on a soft hingeless rotor leading to a 72% reduction of the vibratory loads. However, the advantage of using a gurney flap compared to a trailing edge flap is on the amount of energy required for the actuation and the ease of the implementation of the gurney flap.

A further computational study conducted by Yeo (2008) tried to assess active control mechanisms for rotor performance enhancement. A four-bladed rotor was considered at medium ($80kt$) and high ($150kt$) speed forward flight cases and the gurney flap was assumed to be either completely deployed or retracted. A significant increase in thrust for a given power was found when the gurney was extended from 60%R up to 100%R and activated at the retreating side, which agrees with the outcome of the study by Cheng and Celi (2005) who defined the optimum 2-per-revolution inputs in order to improve the rotor performance by either increasing the thrust of the rotor or decreasing the torque requirement. However, the positive effect of the gurney was observed at medium speed flight while at high speed the performance improvement diminished.

Finally, Gagliardi and Barakos (2009) studied a low twist hovering rotor and the effects of trailing-edge flaps on its performance. A flap located inboard resulted in hover performance similar to a blade of 6 deg more twist. At the same time, a reduction of the trim angles was observed. A flap located outboard did not improve the performance of the rotor although by carefully optimising its configuration similar trim benefits as for the inboard flap were achieved.

The majority of the previous studies are computational and there is a need for experimental investigations of gurney flaps on rotors. This is in contrast to integrated trailing edge flaps that are well-studied using CFD and wind tunnels. For such flaps, in addition to integrated loads, flow fields are also available from techniques like particle image velocimetry (PIV) for fixed and actuated configurations, as reported by Sterenborg et al. (2014). There is, however, an experimental and computational study of the aeromechanics of a Sikorsky demonstration rotor by Lorber et al. (2012) that examined the effect of an active flap. The report points out that the gurney flap may have similar effect to a conventional flap. However, because of its small size the gurney has the potential for high bandwidth active control with low actuation power requirements and minimal impact to the blade structure when compared to conventional control surfaces.

To conclude, few complete studies concerning gurney flap implementation on helicopter rotors were found in the literature. All of them investigated the effect of gurneys on BVI and vibration reduction in forward flight. Although there is strong indication from 2D calculations of potential performance enhancement the question still remains whether there is a practical hover benefit to be achieved or not. In this work, a gurney flap is studied on the main rotor

blade of the W3 Sokol helicopter. The enhancement of the performance is investigated by coupling fluid and structure calculations taking into account the structural properties of the main rotor blade (MRB). The method used for the CFD-CSD coupling was presented in detail in the previous studies of aeroelastic rotors by Dehaeze and Barakos (2012a,b, 2011). To the author's knowledge, there are no studies for the effect of the gurney flap in hover with trimmed, aeroelastic methods and CFD for any real rotor blade.

2. Numerical Methods

2.1. HMB2 flow solver

The Helicopter Multi-Block 2 (HMB2) CFD code Barakos et al. (2005), Steijl et al. (2006), and Steijl and Barakos (2008b) was employed for this work. HMB2 solves the Navier-Stokes equations in integral form using the arbitrary Lagrangian Eulerian formulation for time-dependent domains with moving boundaries:

$$\frac{\mathrm{d}}{\mathrm{d}t}\int\limits_{V(t)} \vec{w} dV + \int\limits_{\partial V(t)} (\vec{F}_{\mathrm{i}}(\vec{w} - \vec{F}_{\mathrm{v}}(\vec{w})\vec{n} dS = \vec{S}. \tag{1}$$

The above equations form a system of conservation laws for any time-dependent control volume $V(t)$ with boundary $\partial V(t)$ and outward unit normal $\vec{n}$. The vector of conserved variables is denoted by $\vec{w} = [\rho, \rho u, \rho v, \rho w, \rho E]^T$, where ρ is the density, u, v, w are the Cartesian velocity components and E is the total internal energy per unit mass. $\vec{F}_{\mathrm{i}}$ and $\vec{F}_{\mathrm{v}}$ are the inviscid and viscous fluxes, respectively. For hovering rotors, the grid is fixed, and a source term, $\vec{S} = [0, -\rho\vec{\omega} \times \vec{u}_{\mathrm{h}}, 0]^T$, is added to compensate for the inertial effects of the rotation. $\vec{u}_{\mathrm{h}}$ is the local velocity field in the rotor-fixed frame of reference.

The non-inertial frame of reference used here has two benefits over a rotating frame of reference: (i) the energy equation is unchanged by the rotation vector $\vec{\omega}$ and (ii) a vanishing 'undisturbed' velocity field occurs in contrast to the position-dependent 'undisturbed' velocity field in the rotating frame of reference, which is given by $-\omega \times \vec{r}$.

Equations (1) are discretized using a cell-centred finite volume approach on structured multiblock grids. The spatial discretisation leads to a set of equations in time,

$$\frac{\partial}{\partial t}(\vec{w}_{\mathrm{i,j,k}} V_{\mathrm{i,j,k}}) = -\vec{R}_{\mathrm{i,j,k}}(\vec{w}_{\mathrm{i,j,k}}), \tag{2}$$

where $\vec{w}$ and $\vec{R}$ are the vectors of cell variables and residuals, respectively. Here, i,j,k are the cells indices in each of the grid blocks, $V_{\mathrm{i,j,k}}$ is the cell volume. The convective terms are discretized using Osher's upwind scheme by Osher and Chakravarthy (1983). MUSCL variable interpolation is used to provide third-order accuracy and the Van Albada limiter by Albada et al. (1982) is employed to prevent spurious oscillations near steep gradients. Boundary conditions are set using ghost cells on the exterior of the computational domain. For viscous flow simulations, ghost values are extrapolated at solid boundaries ensuring that the velocity takes on the solid wall velocity. Implicit time integration is employed, and the resulting linear system of equations is solved using a pre-conditioned Generalised Conjugate Gradient method. For unsteady simulations, an implicit dual-time stepping method is used, based on the pseudo-time integration approach by Jameson (1991). The HMB2 method has been validated for a range of rotorcraft applications and has demonstrated good accuracy and efficiency for very demanding flows. Examples of work with HMB2 can be found in references Steijl et al. (2006), Steijl and Barakos (2008a), and Steijl and Barakos (2008b). Several rotor trimming methods are available in HMB2 along with a blade-actuation algorithm that allows for the near-blade grid quality to be maintained on deforming meshes Steijl et al. (2006).

The HMB2 solver has a library of turbulence closures including several one- and two- equation turbulence models and even non-Boussinesq versions of the $k-\omega$ model. Turbulence simulation is also possible using either the Large-Eddy or the Detached-Eddy simulation approach. The solver was designed with parallel execution in mind and the MPI library along with a load-balancing algorithm are used to this end. For multi-block grid generation, the ICEM-CFD Hexa commercial meshing tool is used and CFD grids with 40-50 or more million points and thousands of blocks are commonly used with the HMB2 solver.

2.2. Modelling gurney Flaps

Recently, the solver was extended to allow for overset grids, and separate to that, functionality to allow for trailing edge flaps has also been presented by Steijl et al. (2010). For the purposes of this study the gurney flap on the W3-Sokol MRB is modelled by flagging any cell face within the computational mesh occupied by the flap with a solid, no-slip boundary condition. This method is implemented in the HMB solver and has been proved to be simple and effective by Woodgate and Barakos (2012). In this case the gurney is

assumed to be thin, and is modelled along a block boundary. The same grid can be used for different size flaps as well as allowing unsteady deployment of gurney flaps along block interfaces. To be able to obtain the loads on the gurney flap alone and to be able to find its moment about a different point - for example the gurney hinge - HMB2 requires some additional information. This is done in two places. Firstly, a special boundary condition tag must be used for the gurney flap to be identified. Secondly, additional input files must be used to define that computations are to be performed with a gurney flap. The advantage of this method is that no additional effort is needed in terms of mesh generation. The results of the method were presented by Woodgate and Barakos (2012).

2.3. Coupling with Structural Dynamics and Trimming

For aeroelastic cases NASTRAN was employed for calculating the static structural deformation of the blade that is modelled as a beam. The main structural properties needed for this analysis are the distributions of the sectional area, the chordwise and flapwise area moments of inertia, the torsional stiffness, and the mass distribution along the span. The W3 MRB was modelled, as presented by MSC Software Corporation (2005), by 29 CBEAM elements along the span and the properties were obtained by PZL Swidnik. At the root, the blade was free to flap but the lead-lag and pitching motion was not allowed. The twist of the blade was linear, $-10.6^o/R$. To account for fluid/structure coupling the aerodynamic loads are extracted from the fluid solution and used in NASTRAN as nodal forces to obtain the deformed blade shape. The blade along with the mesh is deformed based on the structural shape using a method described by Dehaeze and Barakos (2012b). This method first deforms the blade surface using the constant tetrahedral volume (CVT) method. Then it obtains the updated block vertex positions via spring analogy (SAM) and finally it generates the full mesh via a transfinite interpolation (TFI). The same process is repeated until the loads extracted from the flow solution are converged.

A hover trimming method based on blade-element aeroelasticity was used for this study and was described by Steijl et al. (2006). The method requires the lock number γ_{L} of the blade and computes an initial trim state for a hovering rotor. After estimating the collective angle θ based on the thrust coefficient, the lift slope factor of the blade section, and the solidity of the rotor, the inflow factor λ is estimated, as well as the coning angle β. HMB2

is subsequently used to compute the thrust coefficient at this particular trimming before updating the collective and the coning based on the difference between the target and the estimated thrust coefficients. The procedure consists of the following steps:
1. At start-up two options can be used:
(i) an initial estimate of the trim state is computed using the following equation for the collective pitch:

$$\theta_0 = \frac{6}{\sigma\alpha} C_\mathrm{T} + \frac{3}{2}\sqrt{\frac{C_\mathrm{T}}{2}}. \tag{3}$$

(ii) a user defined initial guess for θ_0 is used.
The inflow factor λ can be obtained directly from the equation:

$$\lambda = -\sqrt{\frac{C_\mathrm{T}}{2}} = -\frac{\sigma\alpha}{16}[\sqrt{1 + \frac{64}{3\sigma\alpha}\theta_0} - 1]. \tag{4}$$

For a twisted rotor blade Equation (4) gives the collective pitch at 0.75 of the rotor radius R. Then the equation for the coning angle is used:

$$\beta_0 = \frac{\gamma}{8}[\theta_0 + \frac{4}{3}\lambda]. \tag{5}$$

2. The mesh is subsequently deformed to account for the new rotor blade incidence and position.
3. A steady flow simulation is performed until a prescribed level of convergence is reached.
4. The collective is updated using the following relation:

$$\delta\theta_0 = \frac{C_\mathrm{T,target} - C_\mathrm{T}}{\mathrm{d}C_\mathrm{T}/\mathrm{d}\theta_0}, \tag{6}$$

$$\frac{\mathrm{d}C_\mathrm{T}}{\mathrm{d}\theta_0} = \frac{\sigma\alpha}{6}[1 - \frac{1}{\sqrt{1 + (64/3\sigma\alpha)\theta_0}}]. \tag{7}$$

Equation (5) gives the coning angle for the new collective pitch $\theta_0 + \delta\theta_0$.
5. Steps 2-4 are repeated until a constant trim state is reached.
Therefore, the coning angle β_0 depends on the Lock number and the reduced model assumptions, while the collective is independent as only the derivation of the Newton iteration is dependent on the reduced aerodynamic model.

3. Hover Flight Calculations

3.1. W3-Sokol MRB Geometry

The W3-Sokol main rotor consists of four blades made out of fibre-glass. It is a soft blade in torsion that encourages the idea of the implementation of a gurney flap in order to alter the twist distribution along the radius of the blade. Fig. 1 presents the geometry of the original MRB. The radius of the blade is along the x-axis and the leading-edge points towards the positive y-axis as the blade is rotating counter-clockwise. Although different sections of 5-digit NACA series are used along the radius, the basic section is the NACA23012M which is created by taking some camber out of the baseline NACA23012. At $0.678R$ of the blade there is a trim tab of $0.1c$ length and $0.07R$ span, while from $0.75R$ and up to the blade tip there is a trailing edge tab of $0.05c$. The tip of the blade is rounded as shown in Fig. 1-III(upper panel). The MRB has a blunt trailing edge. All these geometrical characteristics increased the complexity of the generated mesh. Adding a fixed gurney within the multiblock mesh topology would increase the number of nodes and would require additional computational cost to calculate even a steady hover case. For this reason the implementation of a infinitely thin gurney flap was essential. For hover a gurney flap of $0.01c$ was initially located at $0.46R$. The span of the gurney was $0.2R$ and its location and geometry are presented in Fig. 1-II(upper panel). The gurney flap was flagged using the local mesh around the blade. This allows a normal to the trailing edge flap of infinite thickness to be simulated (Fig. 1(lower panel)). The process is described by Woodgate and Barakos (2012).

The mesh used for the hover calculations consists of 5.8 million nodes. A mesh convergence study suggested that this large number of cells was needed for the blade-loads to converge. It is a combined C-type topology in the y-plane with 402 nodes along the blade and O-type topology in the x-plane with 196 nodes around every section of the blade. In the normal direction of the blade 64 nodes have been used. The domain is split in 1360 blocks and it is presented in Fig. 2. For the 4-bladed W3-Sokol rotor, the periodicity boundary condition in space and time is applied in a sector of $2\pi/4$ radians. At the farfield, the inflow, and the outflow surfaces the Froude condition for hover, presented by Wake and Baeder (1996), was applied. The farfield was located 52 chords away from the tip of the blade, while the inflow and outflow boundaries are located 30 and 60 chords away from the blade, respectively.

3.2. Rigid Blade Computations

3.2.1. Performance

Comparative performance calculations have been conducted at six different thrust targets for the rigid clean blade using the $k-\omega$ SST turbulence model. The collective and coning angles used at every case are presented in Table1. The maximum FM was 0.74 and it was observed at medium thrust settings ($C_{\mathrm{T}}/\sigma = 0.185$). At the same setting the torque coefficient was $C_{\mathrm{Q}} = 0.001$. The hover performance for the clean blade as well as the blade with gurney flaps can be seen in Figs. 3 and 4, and an enlarged view is presented in Fig. 5. Three vertical lines are also drawn in that figure corresponding to estimated weight cases for a typical helicopter like the W3 Sokol. In fact, the green line represents hover data provided by PZL Swidnik in order to validate the CFD methods. As demonstrated in Fig. 6a about 200,000 iterations were needed for a well converged solution. If the trimmer was also employed, it added an additional number of iterations since after every retrim the flow needs to adjust and further steps to converge.

3.2.2. Analysis of Rigid Blade Results

In Fig. 7a the surface pressure coefficient is presented and in Fig. 7b the C_{P} plots at three different sections for the clean blade can be seen. The $r/R = 0.56$ station is where the gurney flap will be located, while in the $r/R = 0.73$ section the expected effect of the blade trim tab is observed. The trailing edge tab seems to have a similar effect, which can be seen from the pressure distribution at $r/R = 0.89$. In Fig. 8a the wake of the blade is visualised using the vorticity magnitude of $0.1s^{-1}$, which shows that the vortex created at the tip of the blade interacts with the following blade at near 0.89R, due to the wake contraction. After calculating the performance of the W3 rotor in hover, a gurney flap of 0.2R span was implemented at r/R=0.46 of the blade. The height of the flap varied from 0.3%c up to 2%c and the flap was assumed to be infinitely thin. Hover calculations were conducted for six thrust settings and the HMB2 trimmer was used to force the blade to reach the same thrust as the clean blade. It is pointed out that the gurney improves the performance of the rotor above medium thrust ($C_{\mathrm{T}}/\sigma = 0.185$). The most beneficial gurney size is 2% of the chord and the maximum benefit in figure of merit was +0.044 at $C_{\mathrm{T}} = 0.0154$ ($C_{\mathrm{T}}/\sigma = 0.216$) which corresponds to 6.3% increase compared to the clean case. These results can be seen in Fig. 3. The gurney effect on the wake of the blade is well captured and it is presented in Fig. 8b using the isosurface of vorticity magnitude equal

to $0.1s^{-1}$. For the clean case only the vortices created by the trim tab and the tip of the blade are obvious, while on the blade with the fixed gurney the vortex generated due to the flap is observed inboard. In Fig. 9(a-d) the pressure coefficient on the blade surface is presented for the blade with and without a gurney flap. The effect of the flap on the decrease of the pressure on the suction side and the increase of the pressure on the pressure side is clear, although this effect decays rapidly away from the tips of the flap. A further comparison is conducted between the sectional pressure coefficients of both blades in Fig. 10. It shows that a gurney of $2\%c$ alters the pressure distribution at almost 80% of the sectional surface. At lower thrust where the collective of the blade is not very high the gurney extends more out of the boundary layer and creates additional drag leading to a decrease of the blade performance.

3.3. Aeroelastic Calculations

3.3.1. Application of the Aeroelastic Method and Trimming

Given the sectional properties of the blade, aeroelastic calculations were conducted at the same thrust settings. In Fig. 11 the blade is modelled using beam elements in NASTRAN to calculate the deformed shape according to the loads extracted from the flow solution. The structural properties of the blade are presented in Fig. 12 which suggests that this blade is soft if compared to more modern designs. Especially, the beamwise and the torsional stiffness are very low compared to the chordwise stiffness along the radius which allows the blade to flap and to twist more during flight. The process of getting the final converged solution is summarised in Fig. 6b. Having obtained the converged solution for the rigid blade the aerodynamic loads along the blade are extracted and NASTRAN is used to obtain the new deformed shape using a non-linear analysis (SOLxyz). The mesh is then deformed according to that shape and the flow-field is updated until convergence. The trimmer is then employed to reach the required thrust coefficient and the same process is repeated until the loads converge.

3.3.2. Analysis of Elastic Blade Results

The black dots in Figs. 3 and 4 correspond to the aeroelastic calculations performed for the W3 MRB and the performance of the blade is improved. The agreement between the estimated FM and this of tests is also better. The reason for the aerodynamic enhancement is partly due to the structural properties of the blade which allow some twist, and as a consequence, the

higher twist leads to a higher figure of merit in hover as mentioned in studies by Keys et al. (1987), and by Gagliardi and Barakos (2009). In Fig. 13 the effect of the gurney flap on the sectional thrust, pitching moment, and torque coefficients is presented at the point where the maximum positive effect was captured. These curves were drawn using the aerodynamic loads extracted at 100 different sections along the MRB. The filled squares and the open circles correspond to the loads applied on the nodes used in the structural model. The gurney increased the sectional thrust locally near its location, but the integrated average thrust remained the same due to trimming. As far as the torque is concerned, the gurney flap decreased the requirements more. At the same time the gurney flap introduced more nose-down moments which tend to lower the collective by more than 1 degree as presented in Fig. 17. Although the collective of the blade was further decreased by using a gurney the overall thrust capability of the blade was maintained as extra lift was provided by the flap. This can be also explained in Fig. 18 which shows the comparison of the lift over drag ratio for a clean NACA23102 and for the same aerofoil with a fixed gurney at different incidence. Finally, in Fig. 16 the change of the twist for both the clean blade and the blade with a gurney flap is presented to justify the positive aerodynamic effect of the gurney by further increasing the twist by 1.2 degrees. These results correspond to the hover case where the gurney flap had the most beneficial effect ($C_{\mathrm{T}}/\sigma = 0.216$). The corresponding results to the lower and higher thrust cases are presented in Figs. 14 and 15. The effect of the gurney is quantified in Fig. 5. For a given torque requirement it is obvious that using the gurney a higher thrust coefficient can be reached. This C_T increase for the case of flight test data corresponds to a weight increase of 220 kgs.

4. Conclusions and Future Work

In this work the use of a gurney flap was put forward as a means to improve the hover performance of a helicopter rotor. The basic idea is that the flap will be retracted in forward flight and deployed in hover flight only. The W3 Sokol MRB was used in this work due to the availability of the blade shape and structural properties. The maximum FM of the blade did not improve, but at high thrust settings it was enhanced by 6% over the performance of the clean blade. The effect of the gurney flap to pitch the nose of the section down was evaluated with aeroelastic calculations and it was found that the extra lift of the gurney in combination with the extra

blade twist resulted in an increased FM. For further performance improvement a gurney flap of bigger span could be considered. Among different sizes of gurney the one of 2% of the chord was the most effective. In the future, computations using a fuselage are considered and the location of the gurney will be further optimised to maximise blade performance. The interaction of the wake generated by the rotor blade with the fuselage may affect the rotorcraft performance in such a way that a relocation or a change of the gurney size may be essential. In addition, the effect of adding a mechanism for the flap actuation on the blade structural properties should be investigated.

Acknowledgements
The financial support via the IMESCON Marie Curie ITN project (grant agreement number: 264672), the release of the W3 Sokol main rotor blade geometry by PZL Swidnik, and the use of the computing centre TASK of Gdansk, Poland, are gratefully acknowledged.

Case	θ_0 **(deg)**	β_0 **(deg)**	C_{T}
1	4.5 (3.6)	1.5 (0.6)	0.0045
2	7.0 (6.1)	2.5 (1.8)	0.0082
3	10.0 (9.1)	5.0 (4.1)	0.0132
4	11.5 (10.5)	6.0 (5.2)	0.0154
5	14.0 (12.9)	6.2 (5.5)	0.0189
6	16.0 (14.4)	10.0 (8.7)	0.0209

Table 1 – Control angles and target thrust coefficients for the clean W3-Sokol blade and the blade with fixed gurney flap of 2% of the chord (in brackets) in hover.

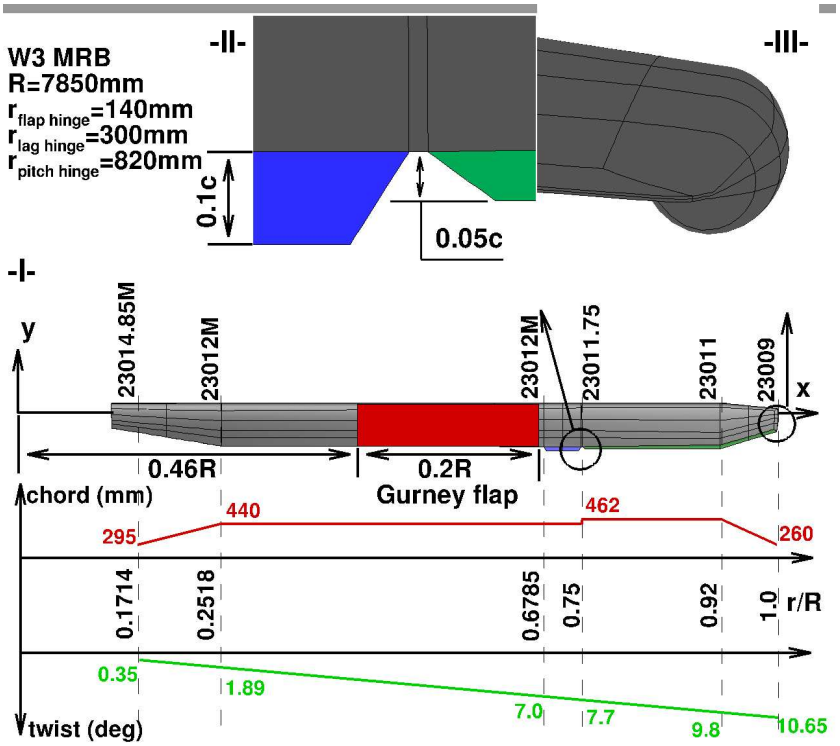

Fig. 1 – (I) Geometry of W3-Sokol MRB, (II) close view at the trim tab and the trailing edge tab, (III) close view at the tip.

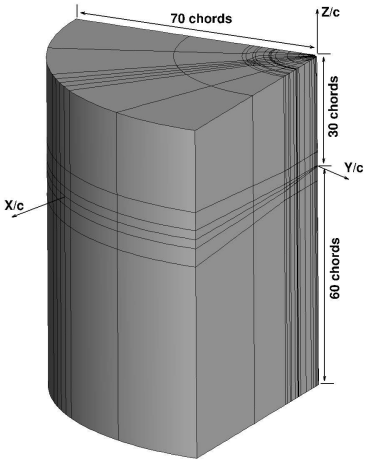

(a)
Multiblock topology for a rotor in hover

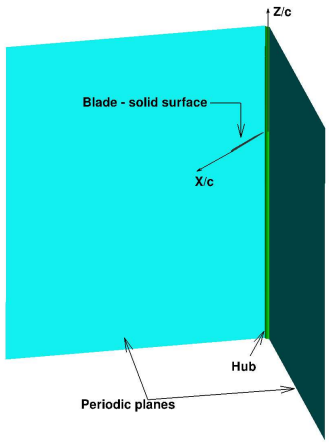

(b)
Detailed view of periodic planes

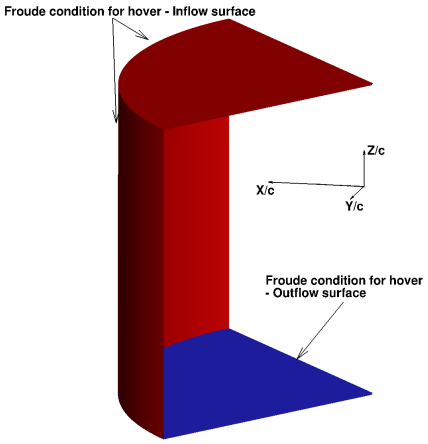

(a)
Detailed view on inflow - outflow conditions

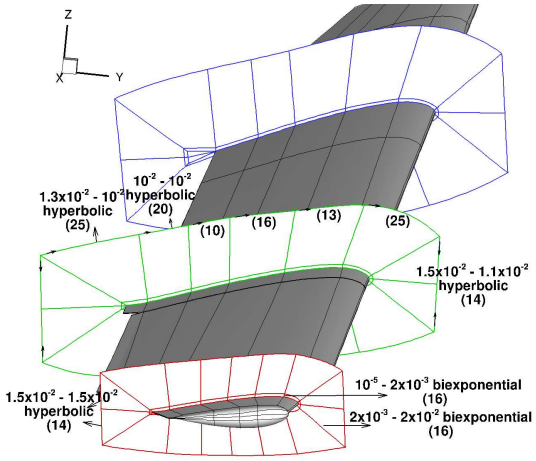

(b)
Blocks around blade in hover.
The numbers in brackets indicate number of nodes on the block edges

Fig. 2 – CFD mesh and boundary conditions on W3 Sokol rotor in hover.

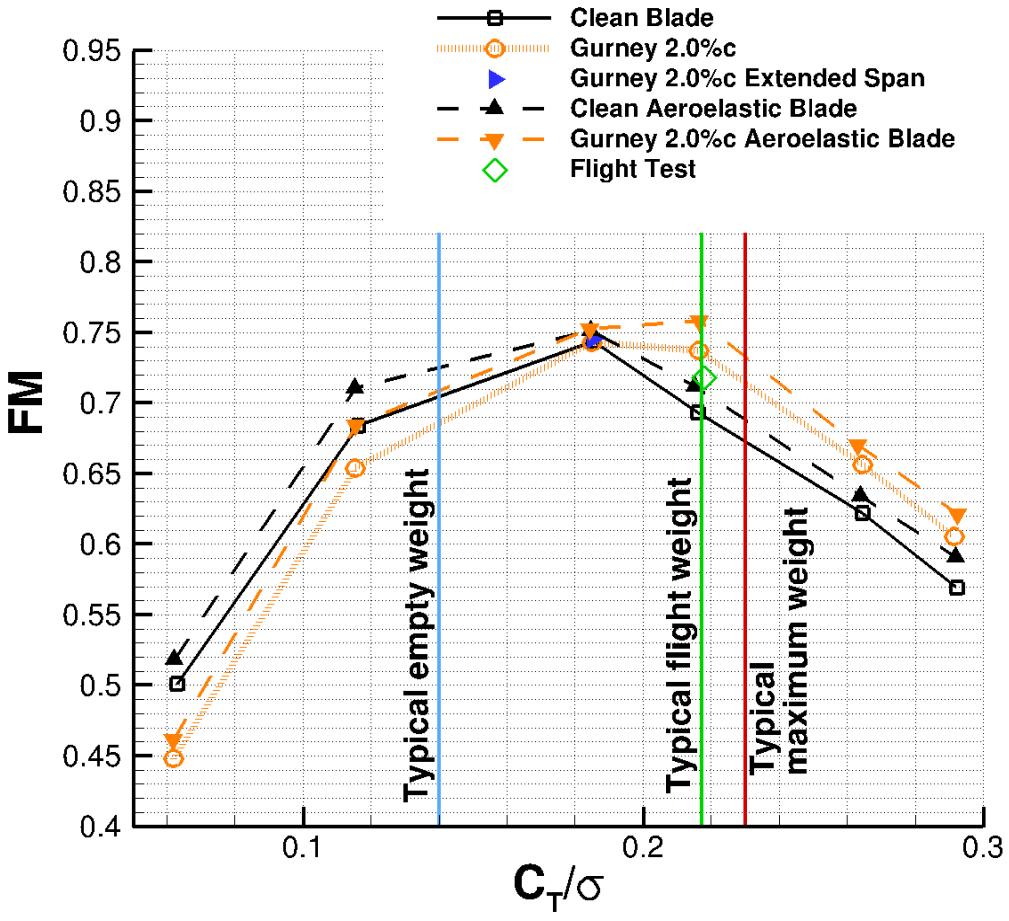

Fig. 3 – Figure of merit versus thrust coefficient for the W3 Sokol MRB in hover ($M_{\text{tip}} = 0.618, \text{Re}_{\text{tip}} = 3.74 \cdot 10^6, \sigma = 0.0714$).

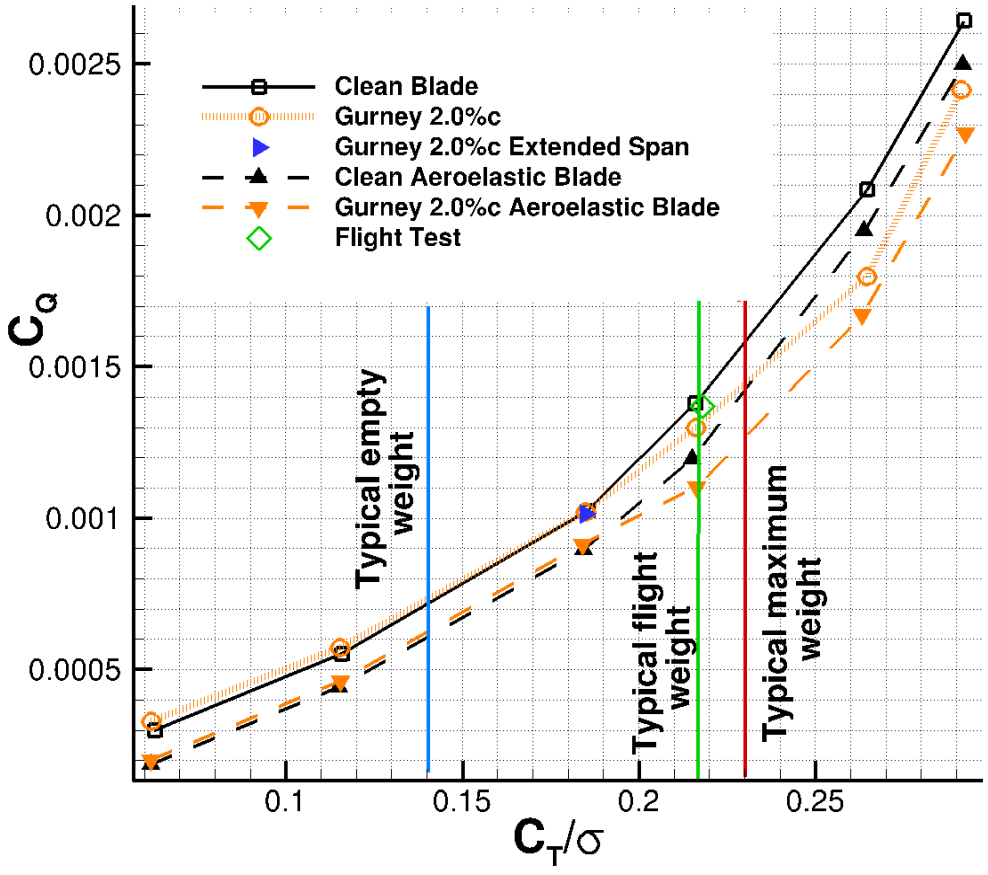

Fig. 4 – Torque versus thrust coefficient for the W3 Sokol MRB in hover ($M_{\text{tip}} = 0.618, \text{Re}_{\text{tip}} = 3.74 \cdot 10^6, \sigma = 0.0714$).

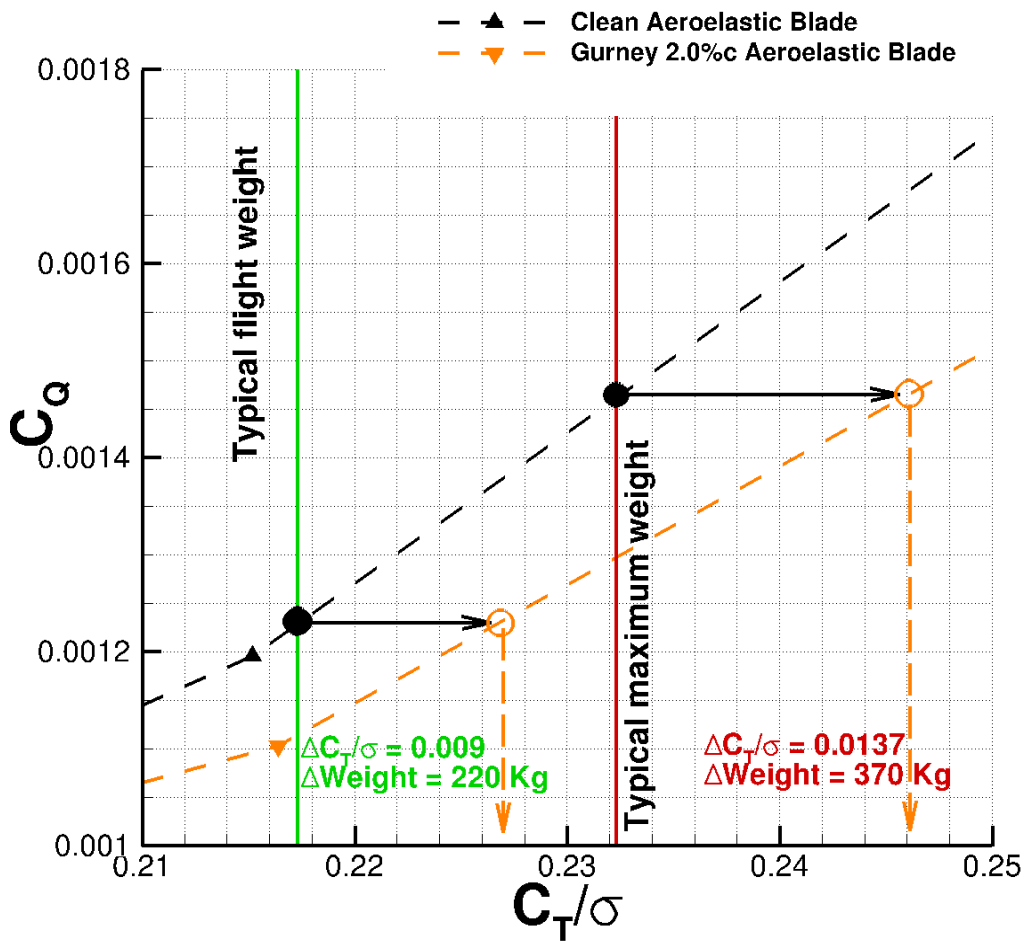

Fig. 5 – Estimated benefit in hover flight when a gurney flap is deployed ($M_{\text{tip}} = 0.618, \text{Re}_{\text{tip}} = 3.74 \cdot 10^6, \sigma = 0.0714$).

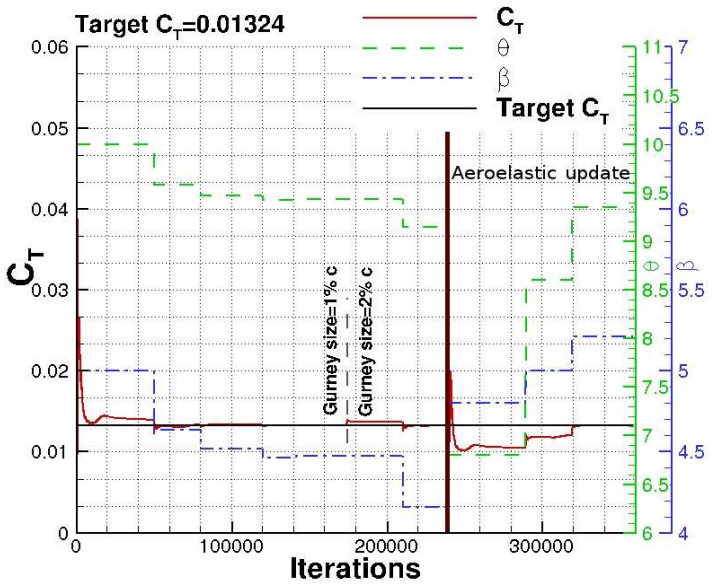

(a)

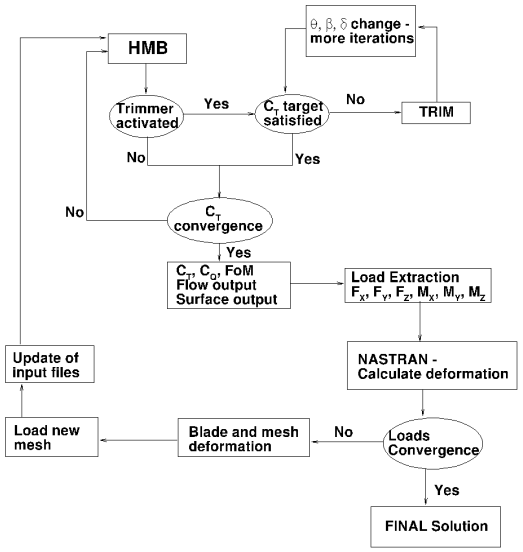

(b)

Fig. 6 – (a) Convergence history for thrust coefficient, collective and coning angle during aeroelastic hover computations along with trimming process. (b) Flow chart for aeroelastic calculations in hover.

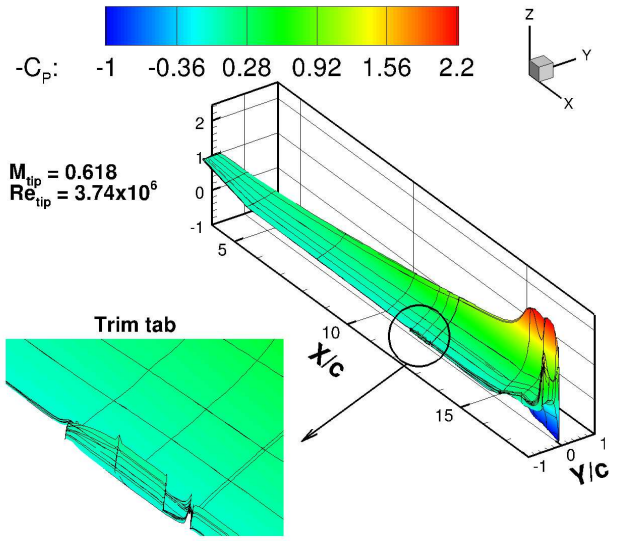

(a)

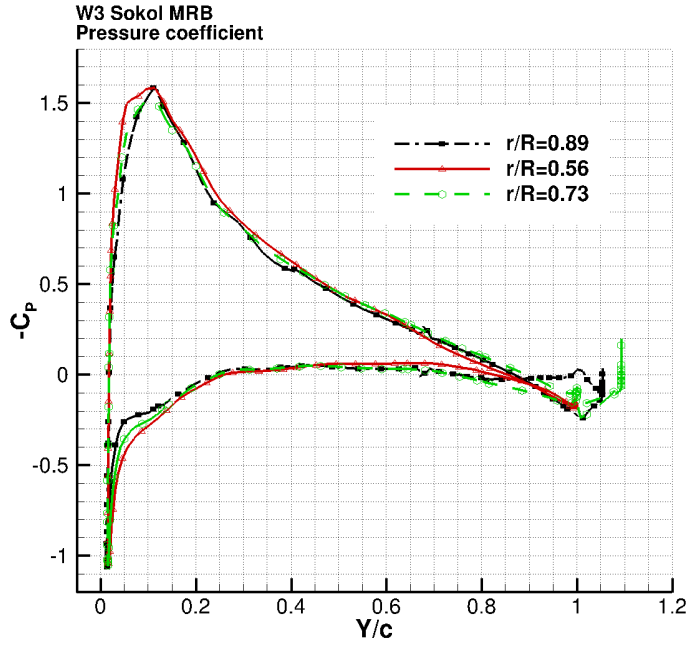

(b)

Fig. 7 – (a) Pressure coefficient along the W3 MRB and (b) pressure coefficient at different sections of the blade normalised using the local dynamic head, $\theta = 10^o$, $\beta = 5^o$, $C_{\mathrm{T}} = 0.0132$, FM $= 0.7432$, $C_{\mathrm{Q}} = 0.001$.

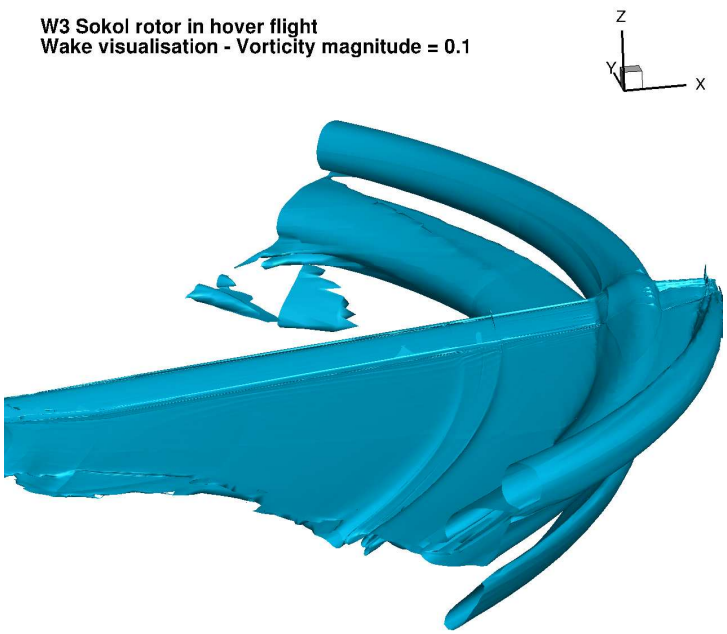

(a)

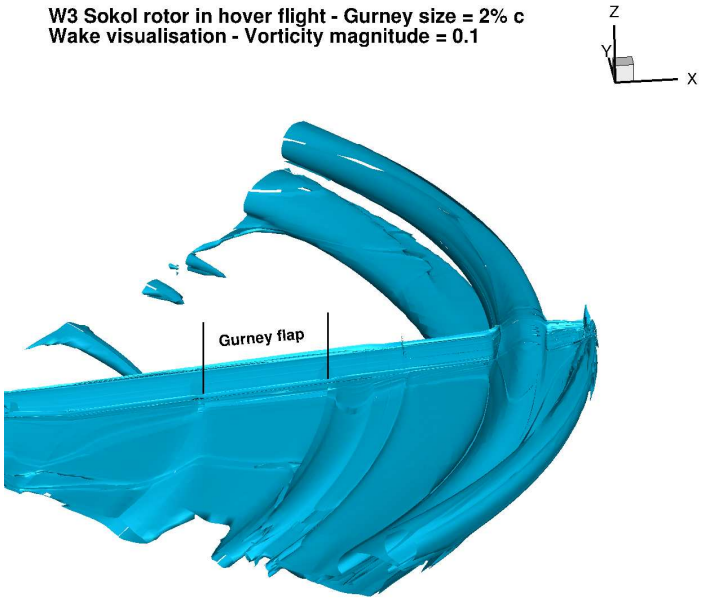

(b)

Fig. 8 – Wake visualisation on W3 MRB (a) with out and (b) with gurney flap in hover by using the isosurface of vorticity magnitude equal to 0.1 s^{-1}, $\theta = 10^o$, $\beta = 5^o$, $C_{\mathrm{T}} = 0.0132$, FM $= 0.7432$, $C_{\mathrm{Q}} = 0.001$.

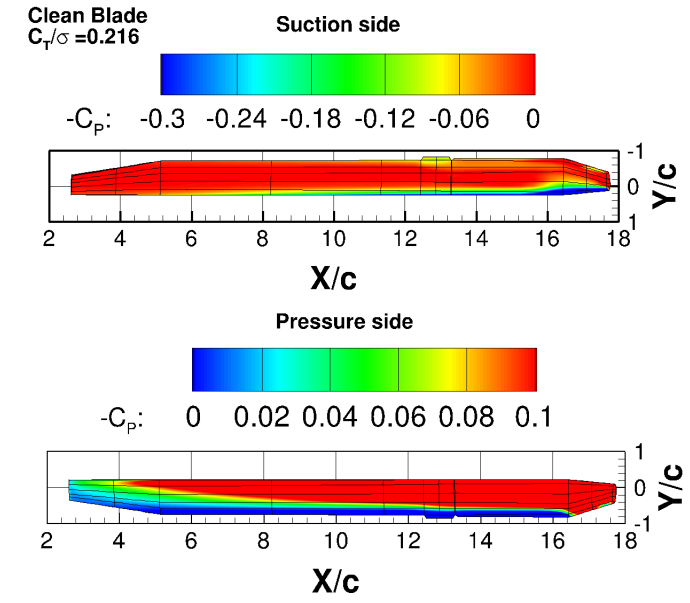

(a) Clean blade

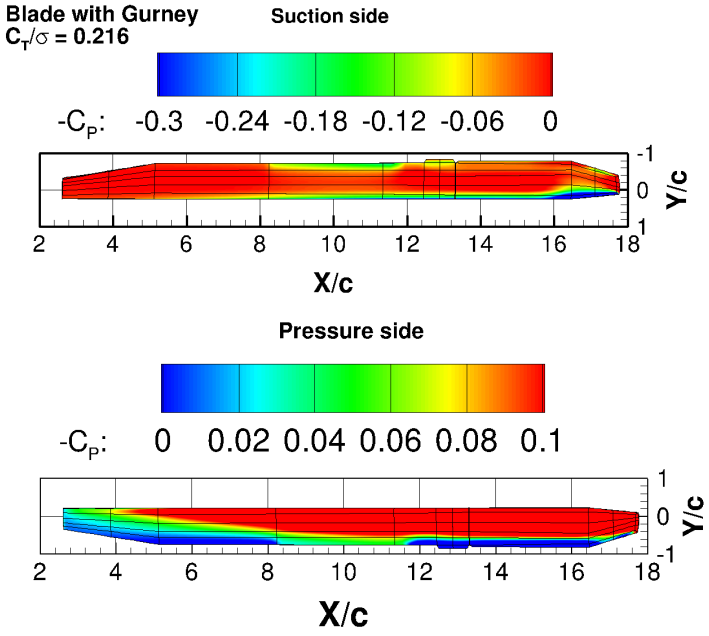

(b) Blade with gurney flap

Fig. 9 – Pressure distribution on upper and lower surface of W3 MRB without gurney (a) and with gurney (b). Clean blade: $\theta = 11.5^o$, $\beta = 6^o$, $C_T/\sigma = 0.216$, FM $= 0.6934$, $C_Q = 0.00138$. Blade with gurney flap: $\theta = 10.46^o$, $\beta = 5.21^o$, $C_T/\sigma = 0.216$, FM $= 0.7374$, $C_Q = 0.00129$.

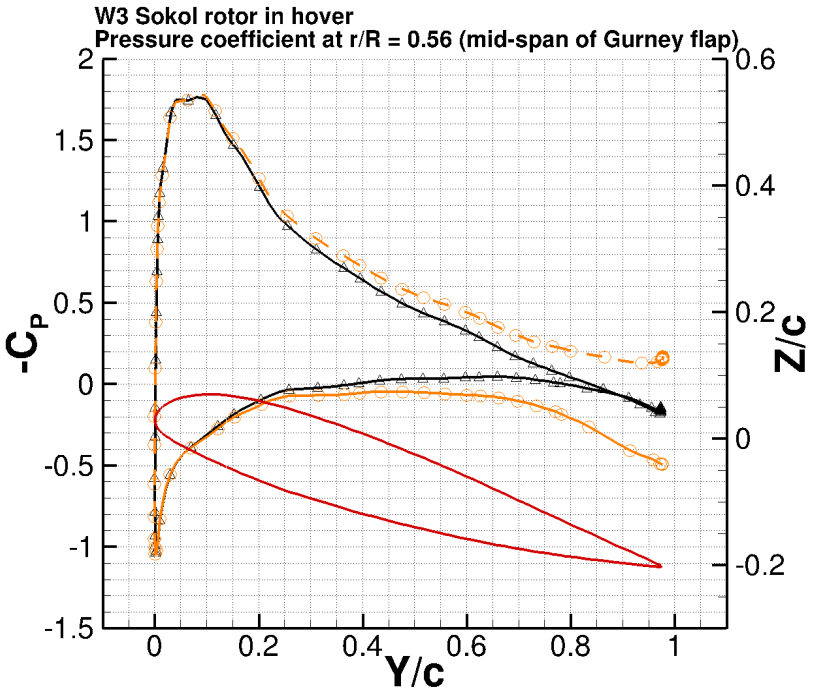

Fig. 10 – Pressure coefficient at $r/R = 0.56$ - Comparison between clean blade and blade with gurney flap.

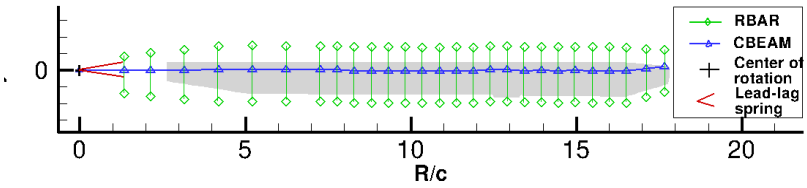

Fig. 11 – Structural model of the W3 Sokol blade used in NASTRAN.

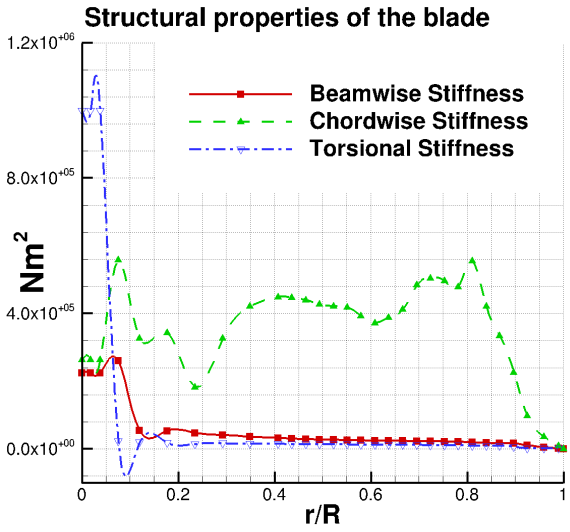

Fig. 12 – Structural properties of the W3 Sokol blade used in NASTRAN.

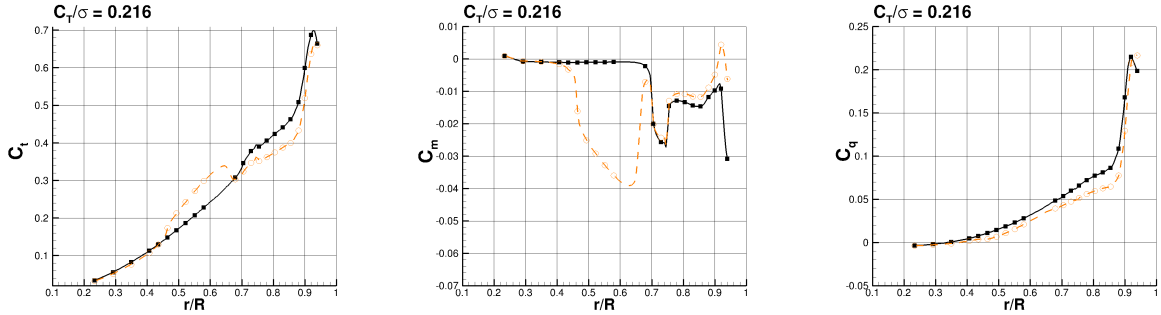

(a) (b) (c)

Fig. 13 – (a) Sectional thrust coefficient, (b) pitching moment coefficient, and (c) torque coefficient of the W3 MRB with (dashed line) and without gurney flap (solid line). Clean blade: $\theta = 11.5^o$, $\beta = 6^o$, $C_T/\sigma = 0.216$, $FM = 0.6934$, $C_Q = 0.00138$. Blade with gurney flap: $\theta = 10.46^o$, $\beta = 5.21^o$, $C_\mathrm{T}/\sigma = 0.216$, FM $= 0.7374$, $C_\mathrm{Q} = 0.00129$.

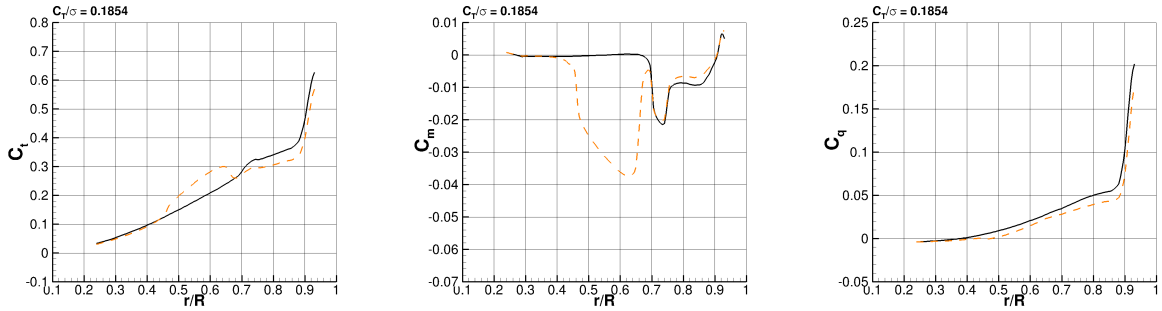

(a) (b) (c)

Fig. 14 – (a) Sectional thrust coefficient (b) pitching moment coefficient, and (c) torque coefficient of the W3 MRB with (dashed line) and without gurney flap (solid line). Clean blade: $\theta = 10.0^o$, $\beta = 5^o$, $C_\mathrm{T}/\sigma = 0.1853$, FM $= 0.7432$, $C_\mathrm{Q} = 0.001$. Blade with gurney flap: $\theta = 9.15^o$, $\beta = 4.16^o$, $C_\mathrm{T}/\sigma = 0.1853$, FM $= 0.7429$, $C_\mathrm{Q} = 0.001$.

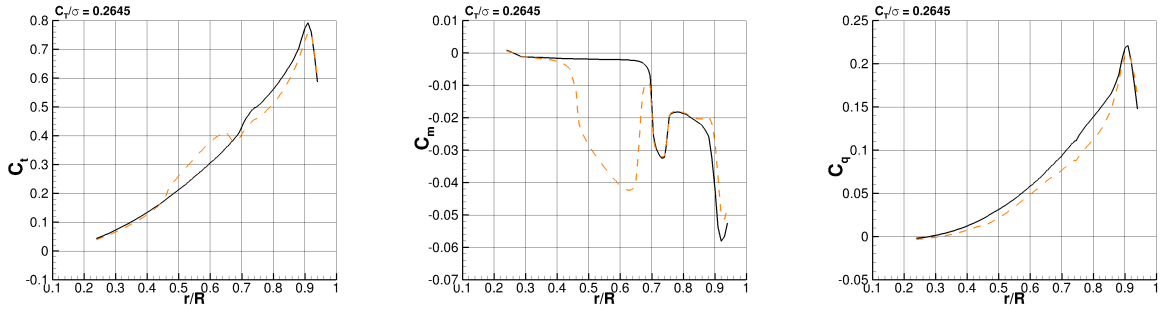

(a) (b) (c)

Fig. 15 – (a) Sectional thrust coefficient, (b) pitching moment coefficient, and (c) torque coefficient of the W3 MRB with (dashed line) and without gurney flap (solid line). Clean blade: $\theta = 14^o$, $\beta = 6.2^o$, $C_\mathrm{T}/\sigma = 0.264$, FM $= 0.622$, $C_\mathrm{Q} = 0.0021$. Blade with gurney flap: $\theta = 12.92^o$, $\beta = 7.36^o$, $C_\mathrm{T}/\sigma = 0.264$, FM $= 0.656$, $C_\mathrm{Q} = 0.0017$.

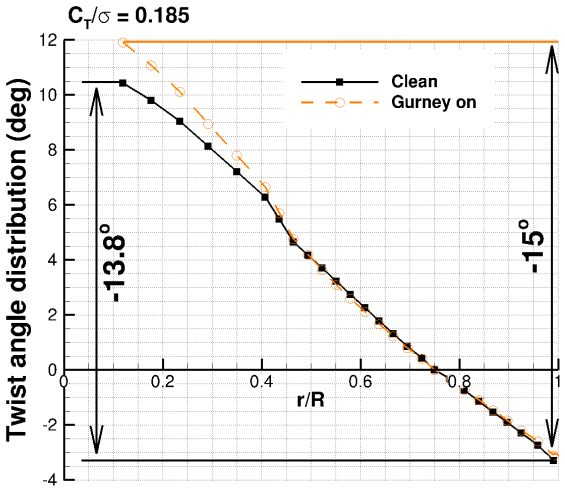

Fig. 16 – Change of twist distribution for W3 MRB with and without gurney flap in hover.

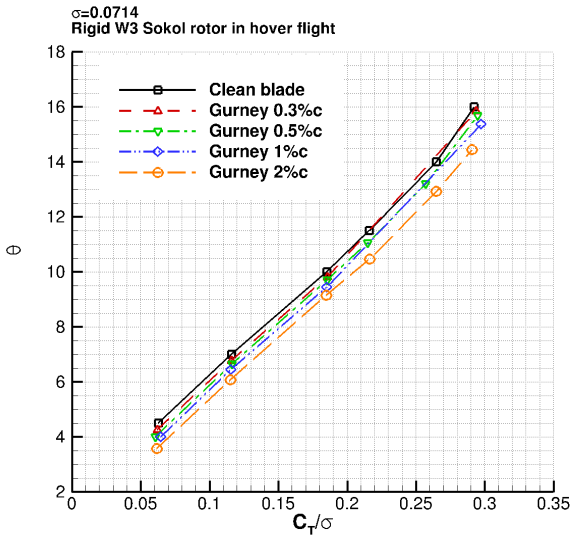

Fig. 17 – Collective angle after trimming versus C_{T}/σ for different gurney sizes on the W3 MRB in hover.

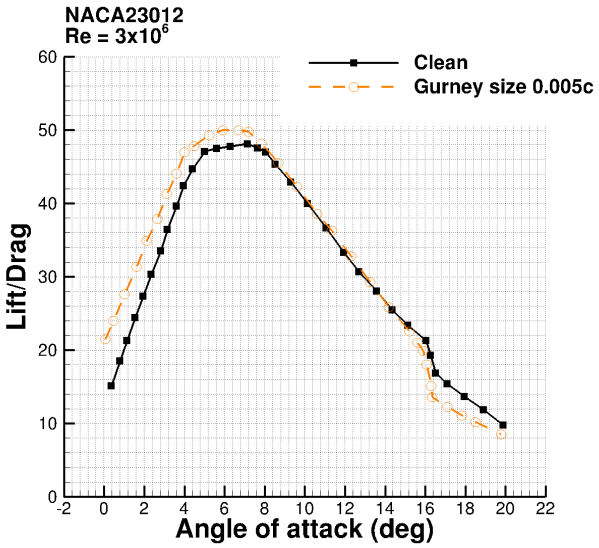

Fig. 18 – Lift over drag comparison for a NACA23012 aerofoil with (dashed line) and without a gurney flap (solid line).

References

Albada, G. D. V., Leer, B. V., Roberts, W., 1982. A comparative study of computational methods in cosmic gas dynamics. Astronomy and Astrophysics 108, pp. 76.

Bae, E. S., Gandhi, F., 2012. Upstream active Gurney flap for rotorcraft vibration reduction 2, pp. 1354–1362.

Baker, J. P., Standish, K. J., van Dam, C. P., March-April 2007. Two-dimensional wind tunnel and computational investigation of a microtab modified airfoil. AAIA, Journal of Aircraft 44 (2), pp. 563–572.

Barakos, G., Steijl, R., Badcock, K., Brocklehurst, A., 2005. Development of CFD capability for full helicopter engineering analysis. In: 31st European Rotorcraft Forum, 13-15 September, Florence, Italy. pp. 91.1–91.15.

Cheng, R. P., Celi, R., 2005. Optimum two-per-revolution inputs for improved rotor performance. AIAA, Journal of Aircraft 42 (6), pp. 1409–1417.

Chow, R., Dam, C. P. V., Sept–Oct 2006. Unsteady computational investigations of deploying load montrol microtabs. AAIA, Journal of Aircraft 43 (5), pp. 1458–1469.

Dehaeze, F., Barakos, G. N., 2011. Aeroelastic CFD computations for rotor flows. In: 37th European Rotorcraft Forum, 13-15 September, Milan, Italy. pp. 143–162.

Dehaeze, F., Barakos, G. N., 2012a. Hovering rotor computations using an aeroelastic blade model. Aeronautical Journal 116 (1180), pp. 621–649.

Dehaeze, F., Barakos, G. N., 2012b. Mesh deformation method for rotor flows. AIAA, Journal of Aircraft 49 (1), pp. 82–92.

Gagliardi, A., Barakos, G. N., 2009. Analysis and design of a flap-equipped low-twist rotor for hover. AIAA, Journal of Aircraft 46 (1), pp. 74–84.

Gai, S. L., Palfrey, R., 2003. Influence of trailing-edge flow control on airfoil performance. AAIA, Journal of Aircraft 40 (2), pp. 332–337.

Jameson, A., 1991. Time dependent calculations using multigrid, with applications to unsteady flows past airfoils and wings. In: 10th Computational Fluid Dynamics Conference, Honolulu, HI. AIAA-91-1596.

Jeffrey, D., Zghang, X., March-April 2000. Aerodynamics of Gurney flaps on a single-element high-lift wing. AIAA, Journal of Aircraft 37 (2), pp. 295–301.

Jeffrey, D., Zhang, X., Hurst, D. W., 2000. Aerodynamics of Gurney flaps on a single-element high-lift wing. AAIA, Journal of Aircraft 37 (2), 295–301.

Keys, C., Tarzanin, F., McHugh, F., 1987. Effect of twist on helicopter performance and vibratory loads. In: 13th European Rotorcraft Forum, Arles, France.

Kinzel, M. P., Maughmer, M. D., Duque, E. P. N., July 2010. Numerical investigation on the aerodynamics of oscillating airfoils with deployable Gurney flaps. AIAA Journal 48 (7), pp. 1457–1469.

Lee, T., Su, Y. Y., 2011. Lift enhancement and flow structure of airfoil with joint trailing-edge flap and Gurney flap. Experiments in Fluids 50, pp. 1671–1684.

Liebeck, R. H., Sept 1978. Design of subsonic airfoils for high lift. AIAA, Journal of Aircraft 15 (9), pp. 547–561.

Liu, L., Padthe, A. K., Friedmann, P. P., July 2011. Computational study of microflaps with application to vibration reduction in helicopter rotors. AIAA Journal 49 (7), pp. 1450–1465.

Lorber, P., Hein, B., Wong, J., Wake, B., 2012. Rotor aeromechanics results from the sikorsky active flap demonstration rotor. In: 68th Annual AHS Forum, AHS International. Vol. 1. pp. 553–568.

Maughmer, M. D., Bramesfeld, G., 2008. Experimental investigation of gurney flaps. AAIA, Journal of Aircraft 45 (6), pp. 2062–2067.

Milgram, J., Chopra, I., Straub, F., 1998. Rotors with trailing edge flaps: Analysis and comparison with experimental data. Journal of the American Helicopter Society 43 (4), pp. 319–332.

Min, B., Sankar, L. N., Rajmohan, N., Prasad, J. V. R., 2009. Computational investigation of gurney flap effects on rotors in forward flight. AIAA, Journal of Aircraft 46 (6), pp. 1957–1964.

MSC Software Corporation, 2005. MSC.Nastran 2005 release guide.

Osher, S., Chakravarthy, S., 1983. Upwind schemes and boundary conditions with applications to euler equationsin general geometries. Journal of Computational Physics (50), pp. 447–481.

Padthe, A. K., Liu, L., Friedmann, P. P., 2011. Numerical evaluation of microflaps for on blade control of noise and vibration. In: Collection of Technical Papers - AIAA/ASME/ASCE/AHS/ASC Structures, 52nd Structural Dynamics and Materials Conference, 4-7 April, Denver, Colorado. AIAA-1873.

Steijl, R., Barakos, G., 2008a. A computational study of the advancing side lift phase problem. AIAA, Journal of Aircraft 45 (1), 246–257.

Steijl, R., Barakos, G., 2008b. Sliding mesh algorithm for CFD analysis of helicopter rotor-fuselage aerodynamics. International Journal for Numerical Methods in Fluids 58, 527–549.

Steijl, R., Barakos, G., Badcock, K., 2006. A framework for CFD analysis of helicopter rotors in hover and forward flight. International Journal for Numerical Methods in Fluids 51 (8), 819–847.

Steijl, R., Woodgate, M., Barakos, G. N., 2010. CFD Method for Efficient Analysis of Flapped Rotors. AHS Specialists' meeting on Aeromechanics, AHS International, 20–22 January, California, USA, pp. 505–517.

Sterenborg, J. J. H. M., Lindeboom, R. C. J., Ferreira, C. J. S., van Zuijlen, A. H., Bijl, H., Feb 2014. Assessment of PIV based unsteady load determination of an airfoil with actuated flap. Journal of Fluids and Structures 45, pp. 79–95.

Tang, D., Dowell, E. H., July-August 2007. Aerodynamic loading for an airfoil with an oscillating Gurney flap. AAIA, Journal of Aircraft 44 (4), pp. 1245–1257.

Troolin, D. R., Longmire, E. K., Lai, W. T., 2006. Time resolved PIV analysis of flow over a NACA 0015 airfoil with Gurney flap. Experiments in Fluids 41, pp. 241–254.

Viswamurthy, S. R., Ganguli, R., 2004. An optimization approach to vibration reduction in helicopter rotors with multiple active trailing edge flaps. Aerospace Science and Technology 8 (3), pp. 185–194.

Wake, B. E., Baeder, J. D., 1996. Evaluation of a navier-stokes analysis method for hover performance prediction. Journal of the American Helicopter Society 41 (1), pp. 7–17.

Wang, J. J., Li, Y. C., Choi, K. S., 2008. Gurney flap - lift enhancement, mechanisms and applications. Progress in Aerospace Sciences 44, pp. 22–47.

Woodgate, M., Barakos, G. N., 2012. Rotor computations with active gurney flaps. 38th European Rotorcraft Forum, 4–7 September, Amsterdam, Netherlands (54).

Yee, K., Joo, W., Lee, D. H., May–June 2007. Aerodynamic performance analysis of a Gurney flap for rotorcraft applications. AIAA, Journal of Aircraft 44 (3), pp. 1003–1014.

Yeo, H., 2008. Assessment of active controls for rotor performance enhancement. Journal of the American Helicopter Society 53 (2), pp. 152–163.